Survey for critical raw materials in Rwanda East African Rift geothermal areas

(https://doi.org/10.5880/GFZ.DMJQ.2026.002)

Franziska D.H. Wilke[1], Leon Ntihabose[2], Eugene Karangwa[2], Jessica A. Stammeier[1], Martin Zimmer[1], Bettina Strauch[1], Samuel Niedermann[1], Simona Regenspurg[1]

1. *GFZ Helmholtz Centre for Geosciences, Potsdam, Germany*
2. *Energy Development Corporation Ltd (EDCL), Kigali, Rwanda*

1. Licence

2. Citation

When using the data please cite:

Wilke, F. D. H.; Ntihabose, L.; Karangwa, E.; Stammeier, J.; Zimmer, M.; Strauch,B.; Niedermann, S.; Regenspurg, S. (2026): Survey of critical raw materials in Rwanda East African Rift geothermal areas. GFZ Data Services. https://doi.org/10.5880/GFZ.DMJQ.2026.002

Table of contents

1. Licence 1
2. Citation 1
Table of contents 1
3. Geology 2
4. Expedition outline and funding 3
5. Summary of results 4
6. Data set and method description 5
Table-A1: sample index 5
Table-A2: Whole rock geochemistry 5
Tables-A3.1–A3.5: Microprobe (EPMA) analyses 6
Table-A4: Results of hydrochemical analysis 6
Table-A5: Results of gas geochemistry 7
Table-A6: Results of noble gas analyses 7
7. Acknowledgements 7
8. References 7

3. Geology

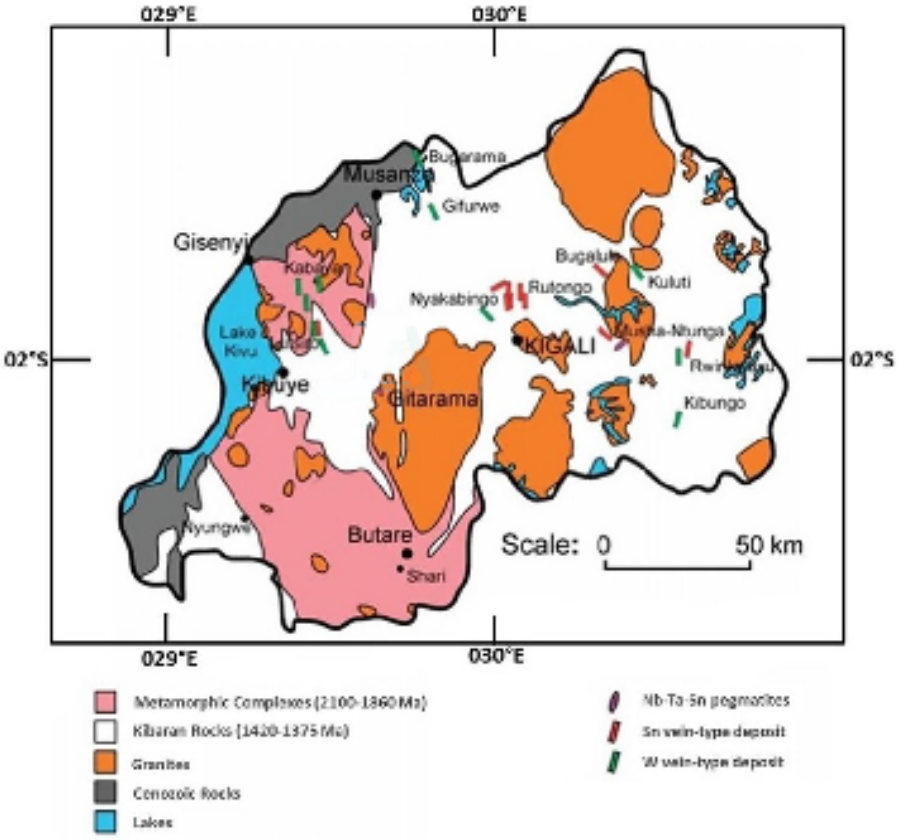

Fig. 1: Geological and structural map of northwestern Rwanda with lake outlines and information about known deposits of critical materials (after Ndikumana et al., 2020).

The East African Rift System (EARS) continues south of the Afar Crossing in Ethiopia through Kenya and then splits into two branches: the western branch, which runs through Uganda and Rwanda, and the eastern branch, which runs through Tanzania. Both unite in Malawi. Magmatic activity began 20 million years ago south of Lake Turkana (Kenya). Here, destabilisation of the continental lithosphere and extrusion of phonolitic floods occurred, and after a phase of resurgence, small-scale ultra-alkaline, Si-saturated activity took place between ca. 5.9 and 2.9 Ma, defining the early rift development and volcanic initiation phase. Volcanism in the western branch of the EARS is confined to four spatially restricted provinces, all of which are found at the tips of long boundary faults or in accommodation zones between rift segments (Ebinger et al., 1989).

The Rwandan sector of the western branch of the East African Rift System is situated within the Albertine Rift and is strongly influenced by magmatic and tectonic processes linked to lithospheric extension, especially in the volcanically active Virunga Volcanic Province, located along its northwestern border. This province forms part of a chain of Quaternary stratovolcanoes associated with significant mantle upwelling and melt generation beneath the rift (Furman & Graham, 1999; Ebinger, 2005). Seismic and tomographic studies indicate pronounced low-velocity anomalies beneath the Virunga segment, reflecting elevated temperatures compared with adjacent rift sectors and partial melt (Shillington et al., 2020).

Rifting in the Albertine domain is generally considered younger than in the eastern branch, with major phases of extension initiating during the Late Cenozoic, commonly estimated at <12 Ma, accompanied by progressive volcanic construction and basin development (Ebinger, 1989; Chorowicz, 2005). Volcanism in the Virunga province has been active from the Late Miocene to Recent, with several edifices remaining historically active, demonstrating sustained magmatic supply (Furman & Graham, 1999).

The Precambrian basement underlying Rwanda is dominated by high-grade metamorphic rocks of the Karagwe-Ankole Belt (formerly described within the NE Kibara Belt), including quartzites, schists, gneisses, and granitoids, representing Palaeoproterozoic to Mesoproterozoic crust accreted along the northwestern margin of the Tanzania Craton (Tack et al., 2010; Fernandez-Alonso et al., 2012; Nambaje et al., 2020). Locally, Archaean orthogneiss domains have been documented, indicating reworked older continental crust (Nambaje et al., 2020). These units are unconformably overlain in places by Neoproterozoic to Phanerozoic sedimentary successions within rift basins. Magmatism in Rwanda is primarily expressed through silica-undersaturated alkaline volcanics, including basanites, tephrites, and nephelinites erupted within the Virunga and South Kivu belts (Furman & Graham, 1999). Rift-related sediments and unconsolidated basin fills occur around Lake Kivu and associated half-grabens.

4. Expedition outline and funding

In autumn 2024, an expedition to Rwanda was undertaken within the framework of the research project "CRM-geothermal". Within „CRM-geothermal", we are looking for an environmentally friendly co-production of critical raw materials together with the provision of geothermal energy. In the EARS, high levels of rare earth elements (REE), Sr, Ba and Mg are expected in waters and solids in areas with alkaline volcanic rocks, while other critical elements, including helium, have been sought in other localities. The eastern and western branches of the EARS host juvenile sectors with promising geothermal potential related to hot fluids migrating along permeable faults.

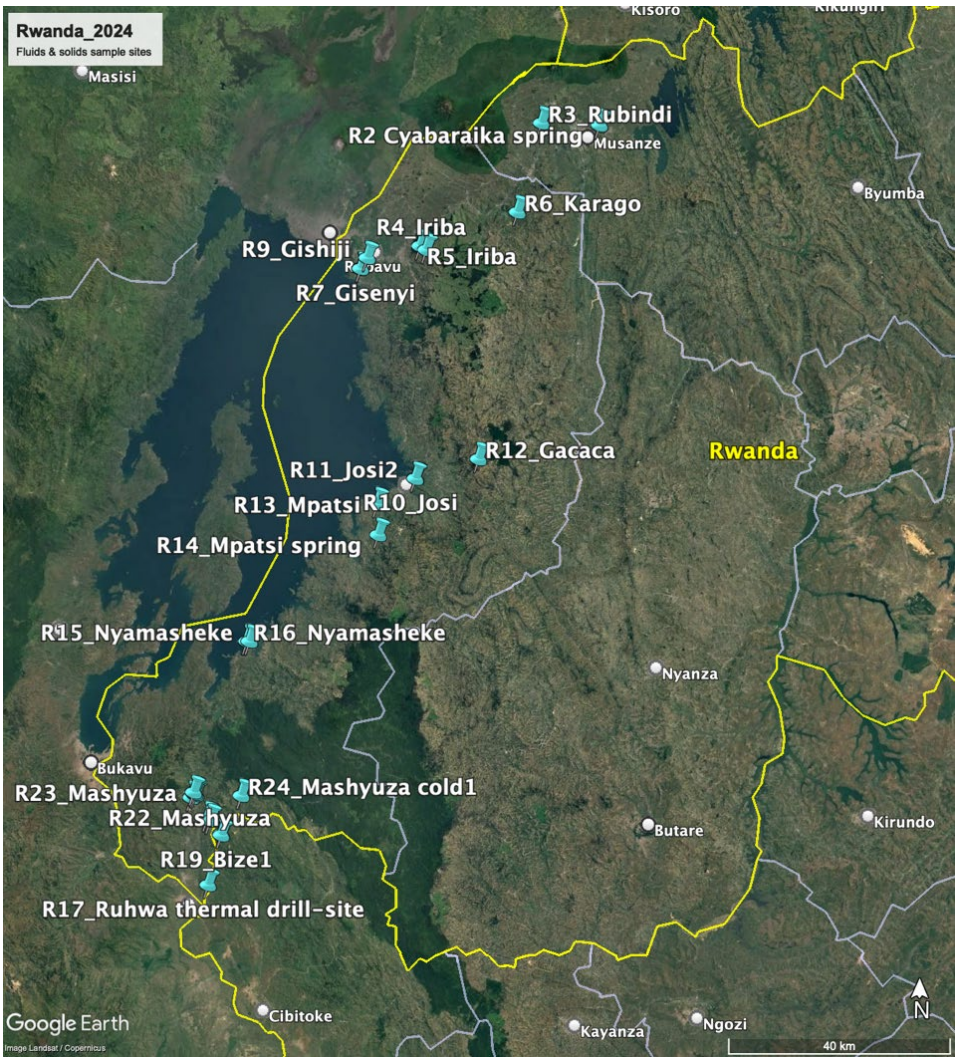

Fig. 2 Map showing sampling locations (turquoise needles). Sampling points close to each other may overlap. GPS data are given in Table A1.

The expedition began in the Virunga Volcanic Province in north-western Rwanda and continued all along Lake Kivu to Kamembe Further, along the Nyakabuye-Ruhwa Valley, in the area of Bugarama, Ruhwa and Mashyuza, gas, water, rock and sediment associated with natural hot springs but also cold springs were collected. On site, physical and chemical parameters were measured in-situ and documented together with the geology, infrastructure and domestic use of the hot site. At Ruhwa borehole, southern Rwanda, the hot water (66°C) emerges as an artesian spring at the surface. Drilling sites for geothermal water and energy extraction in Karisimbi were not visited because no economically viable geothermal system was found. Gisenyi and Bugarama are in the focus of the authorities, but funding for drilling at these sites was not yet achieved. We visited these sites to monitor the physicochemical parameters and to highlight the importance of their usage.

We strongly support the idea of using geothermal water in rural areas and decentralising the energy supply system to make it less prone to disruption. Since both geothermal sites, Gisenyi and Bugarama, are within highly populated areas, direct usage of heat and energy would be of major economic and ecologic advantage, saving wood and charcoal, preventing air contamination and providing energy for light and electric media in private and public properties. That said, there is huge potential to enhance the everyday life of local residence, making the society less prone to influences from outside their quarters, foreign countries and changing climate.

5. Summary of results

In comparison to southern Tanzania, where the noble gas analysis showed a mixed crustal-mantle origin, with helium concentrations reaching up to 7 vol% and $^3He/^4He$ ratios up to 3.4 R_a indicating a clear mantle component (Wilke et al., 2024), the helium concentrations from Rwanda are less spectacular. Still, in Iriba (R4), Karago (R6) and Mpatsi (R13), the most northern/northwestern locations in Rwanda, helium concentrations reach up 2 vol% with $^3He/^4He$ ratios of ~0.09 R_a, ~0.07 R_a and ~0.15 R_a, respectively, indicating a predominantly crustal origin. At the hottest spring locations in Gisenyi (ca. 70°C), up to 0.4 vol% He was measured. Cyabaraika (R1, R2) in the north and Mashyuza (R23) in the south have the highest $^3He/^4He$ ratio of >1.7 R_a. Both geothermal sites are linked to Cenozoic volcanic provinces: the Virunga province in the north and the South Kivu province in the south, both of which are in contact to the Mesoproterozoic Akanyaru supergroup (part of the Kibara Belt).

Water was sampled from hot and cold springs (18-70 °C) at agricultural sites and in urban areas, along a line stretching from Virunga in the north towards, and along, the western shoreline of Lake Kivu, as well as from dried riverbeds, an abandoned borehole and a limestone open pit mining area in southwestern Rwanda, at the border to Burundi. The pH values of the spring waters range from 7.2 to 7.6. Spring water temperatures are a little lower in comparison to Tanzania and Malawi springs (Wilke et al., 2024; 2025). The pH value is neutral and differs from those in Tanzania and Malawi, where waters range from neutral to low alkaline. Sodium is again the major cation. The major anions are sulphate and chlorine, with comparable concentrations to what was found in Malawi and thus tens to hundreds of times lower than in Tanzania.

An elevated concentration of REY was detected in Karago (R6) with almost 210 µg/l. Lithium and germanium are enriched in Bize (R18, R19), Mashyuza (R22, R23) and Josi (R10, R11) with up to 1300 µg/l Li and 15 µg/l Ge. All results are the highest concentrations found so far, also in comparison to Malawi and Tanzania.

Gisenyi has the hottest geothermal springs with surface temperatures of ca. 70°C. Like Karago (R6) and Iriba (R4), both with higher He concentrations, these hot springs arise from Palaeo- to Mesoproterozoic felsic rocks (Fernandez-Alonso et al., 2012). The source rock is a white mica-rich

schist or gneiss, as evident by the host rocks and/or mineral separates occurring at the surface alongside with the geothermal water. In terms of CRMs (He, REY), Karago (R6) is the most interesting site within our survey, though the water temperature is “only” 40°C at the surface.

Regarding the occurrence of lithium and germanium, as mentioned above, both Mashyuza (R23) and Bize (R18, R19) belong to the young South Kivu volcanic province in contact to the Mesoproterozoic Akanyaru supergroup. Josi (R10, R11) geothermal waters are, as well, released from Kibaran metamorphic phyllite, appearing in a ca. 2 km wide valley that is most probably the surface manifestation of a N-S trending fault. In Mpatsi (R13), granites have been found on the agricultural site. This site is located between Mesoproterozoic metamorphic and crystalline rocks.

6. Data set and method description

The data are organised in one Excel file (2026-002_Wilke-et-al_data.xlsx) with ten individual spreasheets. All tables are additionally provided in csv format.

The tables are listing all samples and subsamples as rows and the measured variables as consecutive columns. Table A1 includes an index saying which component (gas, water, solid) of a sample was analysed for what. Table A2 shows the whole rock analyses. A3.1 – A3.5 present the electron microprobe analyses of specific minerals, A4 the water anion, cation and trace element analyses. Table A5 shows the gas geochemistry and A6 the noble gas analyses.

Where material could be sampled in sufficient quantity, it will be stored at the GFZ material repository for further, also external, use.

Table-A1: sample index

Sample ID, date of collection, sample name = location, GPS coordinates, on-site fluid measurement results and on-site notes are given. The geologic structure of the sampling site is given as well as the host rock type from which the samples were taken. The following part of the table has information if a thin section or a whole rock powder is available and which analyses were performed for which component of a specific sample.

Table-A2: Whole rock geochemistry

Laboratory: Elements and Minerals of the Earth Laboratory (ElMiE Lab, GFZ Helmholtz Centre for Geosciences, Germany)

Major and some minor elements were analysed using X-ray fluorescence (XRF) on fused glass beads. For analysis of major and trace elements, fused beads were prepared using dried flux consisting of lithium tetraborate (66%) and lithium metaborate (34%; FX-X65-2, Fluxana GmbH & Co. KG, Germany). Fused beads were measured with an XRF spectrometer (Zetium, Malvern Panalytical, UK) using a Rh tube. Loss on ignition (LOI) was determined by weight difference after fusion. Long term (ca. 2 years) analytical precision is within 5% (1 SD, n=50) for main elements (percent range) and 10% (1 SD, n=50) for minor elements (mg/kg range); determined by regular analysis of three reference materials BM, GM, TB (basalt, granite, and shale powder, respectively; Zentrales Geologisches Institut ZGI, Germany).

Tables-A3.1–A3.5: Microprobe (EPMA) analyses

Laboratory: Microprobe Lab (GFZ Helmholtz Centre for Geosciences, Germany)

EPMA analyses were done on selected samples and minerals only after careful observation of hydrochemical results. The focus was to find host materials for elevated concentrations of lithium, strontium and germanium, such as in R7 Gisenyi, R10 Josi, R17 Rhuwa, R18 & R19 Bize and R22 Mashyuza, in accordance to the geothermal water temperatures.

Analyses of zircon (A3.1), carbonates (A3.2), tourmaline (A3.3), silicate (A3.4) and scales (A3.5) were performed at operating conditions of 10-20kV and 5-40 nA with a focused beam for stable phases like zircon, but with 2-15 µm beam for e.g., tourmaline, oxides, micas and carbonates. Counting times varied between 10 and 30 s on peaks and on background. Synthetic and natural standards were used from international distributors (GEO MK II, Astimex® MAC, Smithsonian Institute). For mica, oxygen equivalents of F and Cl were given after the sum of all wt. %. Such equivalents need to be subtracted from the analytical sum. The oxygen equivalent of F is calculated by multiplying moles of F by 0.4211 and moles of Cl by 0.255. Detection limits (DL) of each element are given at the top head of each table. Please note, these are elemental DL, not those for oxides. Iron is given as Fe^{2+}, where needed Fe^{3+} is stoichiometrically calculated (Fe^{2+} x 1.1113= Fe^{3+}). Cells with "–" = not determined, empty cells do not apply.

Table-A4: Results of hydrochemical analysis

Laboratory: Elements and Minerals of the Earth Laboratory (ElMiE Lab, GFZ Helmholtz Centre for Geosciences, Germany)

Field analysis: The physicochemical parameters, pH value, redox value, electric conductivity, and temperature were measured with two WTW Multi 3630 IDS meters. Carbonate/bicarbonate was determined by titration (carbonate hardness field test).

All fluid samples and blanks including acid blanks were diluted with 2 vol.% HNO_3 using ultrapure reagents and doped online with 1 µl/l indium to correct for sensitivity drift. Dilutions and standard addition were performed online using an auto diluter system (prepFast, Elemental Scientific Inc.). Concentrations were quantified using high-resolution inductively coupled plasma mass spectrometry (ICP-MS, ELEMENT XR, Thermo Scientific, USA).

Trace elements and REE were measured in separate aliquots and separate analytical sessions. Concentrations were each determined by external calibration with a 3-point calibration line using multi-element standards. Acid blanks were measured within the sequence and subtracted online from raw counts. REEs were all measured in high mass resolution mode to avoid isobaric interferences, while the remaining trace elements were measured in the lowest mass resolution possible to maintain high sensitivity while avoiding interferences.

Major cations (Ca, K, Mg, Na and Si) in water samples were determined using a 5110 spectrometer with Vertical Dual View configuration (Agilent, USA). The analytical precision and repeatability were generally better than 2%, which is regularly tested by certified reference material and in-house standards. Samples were diluted with ultrapure HCl. Quantification was performed by standard addition with a three- and five-point calibration using a single element solution Specpure (Thermo Fisher Scientific).

Table-A5: Results of gas geochemistry

Laboratory: Gas Geochemistry Lab (GFZ Helmholtz Centre for Geosciences, Germany)

Gas samples were taken using a funnel-and-tube system, in which gas is collected by sampling bubbles in a glass flask initially filled with spring water, with the gas successively replacing the water in the flask. Sampling was completed (i.e., the stopcocks were closed) when the water was completely evacuated, depending on the gas flow.

The chemical composition of gas samples (H_2, He, N_2, O_2, CH_4, Ar, CO_2) was analysed in the laboratories of the GFZ using an Omnistar (Pfeiffer Vacuum) quadrupole mass spectrometer with closed ion source and a mass range from 1 to 100 amu. Calibration was performed with two certified test gases and air; the relative standard deviation was <10 %. Appropriate splits of the samples were analysed for noble gas concentrations (Table A6).

Table-A6: Results of noble gas analyses

Laboratory: Noble Gas Lab (GFZ Helmholtz Centre for Geosciences, Germany)

To remove the reactive gases (e.g. CO_2, CO, H_2O, N_2, H_2, O_2 and various hydrocarbon compounds), a pipe loop cooled with dry ice, two titanium sponge getters cooled from 750°C to 400°C during the process, one SAES getter with Zr-Al alloy held at room temperature and a second one at 400°C were used. To separate Ar, Kr, Xe from He and Ne, the heavy gases were quantitatively adsorbed to a stainless-steel frit at 50 K in a cryogenic cold head. Helium and neon were trapped at 11 K in another cold head equipped with activated charcoal. The gases were then released at appropriate desorption temperatures and analysed separately in the sequence Ar, Kr+Xe, He, Ne (or Ar+Kr, He, Ne when using the charcoal finger). More details about measurement procedures can be found in Niedermann et al. (1997) and Daskalopoulou et al. (2025).

Noble gas concentrations shown in Table A6 have been calculated assuming a total pressure of 1000 mbar in the sampling flasks; their 2σ uncertainties are estimated at ~10-20%.

7. Acknowledgements

Samples were collected by Franziska Wilke, Leon Ntihabose, Eugene Karangwa, Martin Zimmer and Bettina Strauch during a field campaign in 2024. This expedition took place under the umbrella of the European Union funded project “CRM-Geothermal”, but was financed with GFZ expedition money (grant X-031-22-01). We would like to warmly thank Hartmut Liep for rock crushing and sieving, Heike Rothe for assisting in ICP-MS measurements and Enzio Schnabel for performing the noble gas isotope measurements. Nicolai Klitscher prepared the rock cuttings and polished the thin sections.

8. References

Chorowicz, J. (2005). The east African rift system. Journal of African Earth Sciences, 43(1-3), 379-410. https://doi.org/10.1016/j.jafrearsci.2005.07.019

Daskalopoulou, K., Niedermann, S., Wilke, F. D. H., Zimmer, M., Woith, H., Glodny. J., Geissler, W. H., & Kämpf, H. (2025). Characterisation of deep intra-continental magma reservoirs – Insights from noble gases and p-T estimates into the western Eger Rift (Czech Republic). Chemical Geology, 681, 122722. https://doi.org/10.1016/j.chemgeo.2025.122722

Ebinger, C. J., Deino, A. L., Drake, R. E., & Tesha, A. L. (1989). Chronology of volcanism and rift basin propagation: Rungwe Volcanic Province, East Africa. Journal of Geophysical Research, 94(B11), 15,785–15,803. https://doi.org/10.1029/JB094iB11p15785

Ebinger, C. (2005). Continental break-up: the East African perspective. Astronomy & Geophysics, 46(2), 2-16. https://doi.org/10.1111/j.1468-4004.2005.46216.x

Furman, T., & Graham, D. (1999). Erosion of lithospheric mantle beneath the East African Rift system: geochemical evidence from the Kivu volcanic province. In Developments in Geotectonics (Vol. 24, pp. 237-262). https://doi.org/10.1016/S0024-4937(99)00031-6

Fernandez-Alonso, M., Cutten, H., De Waele, B., Tack, L., Tahon, A., Baudet, D., & Barritt, S. D. (2012). The Mesoproterozoic Karagwe-Ankole Belt (formerly the NE Kibara Belt): The result of prolonged extensional intracratonic basin development punctuated by two short-lived far-field compressional events. Precambrian Research, 216, 63-86. https://doi.org/10.1016/j.precamres.2012.06.007

Nambaje, C., Williams, I. S., Satish-Kumar, M., & Sajeev, K. (2020). Direct evidence for Archean crust in the Western Domain of the Karagwe Ankole Belt, Rwanda: Implications for Neoarchean to Paleoproterozoic crustal evolution. Precambrian Research, 350, 105851. https://doi.org/10.1016/j.precamres.2020.105851

Ndikumana, J. D. D., Bolarinwa, A. T., Adeyemi, G. O., Olajide-Kayode, J., & Nambaje, C. (2020). Geochemistry of feldspar and muscovite from pegmatite of the Gatumba area, Karagwe Ankole Belt: implications for Nb–Ta–Sn mineralisation and associated alterations. SN Applied Sciences, 2(9), 1568. https://doi.org/10.1007/s42452-020-03370-1

Niedermann, S., Bach, W., & Erzinger, J. (1997). Noble gas evidence for a lower mantle component in MORBs from the southern East Pacific Rise: Decoupling of helium and neon isotope systematics. Geochimica et Cosmochimica Acta, 61(13), 2697-2715. https://doi.org/10.1016/S0016-7037(97)00102-6

Shillington, D. J., Scholz, C. A., Chindandali, P. R. N., Gaherty, J. B., Accardo, N. J., Onyango, E., et al. (2020). Controls on rift faulting in the North Basin of the Malawi (Nyasa) Rift, East Africa. Tectonics, 39, e2019TC005633. https://doi.org/ 10.1029/2019TC005633

Tack, L., Wingate, M. T. D., De Waele, B., Meert, J., Belousova, E., Griffin, B., ... & Fernandez-Alonso, M. (2010). The 1375 Ma “Kibaran event” in Central Africa: Prominent emplacement of bimodal magmatism under extensional regime. Precambrian research, 180(1-2), 63-84. https://doi.org/10.1016/j.precamres.2010.02.022

Wilke, F. D., Mahecho, A., Regenspurg, S., Zimmer, M., Jentsch, A., Kreitsmann, T., ... & Stammeier, J. (2024). Survey for critical raw materials in Tanzanian East African Rift geothermal areas. https://doi.org/10.5880/GFZ.3.1.2024.006

Wilke, F., Gondwe, K., Regenspurg, S., Zimmer, M., Strauch, B., Stammeier, J. A., ... & Niedermann, S. (2025). Survey for critical raw materials in Malawi East African Rift geothermal areas. https://doi.org/10.5880/GFZ.DMJQ.2025.001